Indian J Phys (October 2021) 95(10):2187–2199
https://doi.org/10.1007/s12648-020-01870-9

ORIGINAL PAPER

Structure of lead silicate glasses and its correlation with photoelastic properties

A Khanna[1]*, A Kaur[1], M Fábián[2], Hirdesh[1] and A Kaur[1]

[1]Department of Physics, Guru Nanak Dev University, Amritsar, Punjab 143005, India

[2]Center for Energy Research, Konkoly Thege St 29-33, Budapest 1121, Hungary

Received: 14 December 2019 / Accepted: 14 May 2020 / Published online: 17 October 2020

Abstract: Short-range structures of xPbO–(100 − x)SiO_2 (x = 50, 60 and 65 mol%) glasses were studied by neutron diffraction and Reverse Monte Carlo modeling. Si–O atomic pair correlation distributions are symmetrical and show peaks in the range: 1.60–1.64 ± 0.02 Å. Si^{4+} are tetrahedrally co-ordinated with oxygen, whereas the Pb–O and O–O atomic pair correlation distributions are broad and asymmetrical due to the existence of wide range of Pb–O and O–O distances in the glass network. The peak positions in the Pb–O atomic pair correlations shift from 2.60 ± 0.05 to 2.42 ± 0.05 Å on increasing PbO concentration from 50 to 65 mol%. Pb^{2+} exist in PbO_x (x = 3, 4, 5 and 6) structural units, and the average Pb–O coordination is constant and is in the range of 4.08 ± 0.11 to 4.14 ± 0.08. The O–Si–O bond angles distributions are broad and asymmetrical with peak values in the range of 91° to 109°, and deviate significantly from the value of 109.5° in the ideal tetrahedral structural units. The short-range structural properties of glasses i.e. the cation-oxygen coordination numbers and bond lengths were used to predict the photoelastic properties of the glasses by the Zwanziger model, and it is concluded that xPbO–(100 − x)SiO_2 (x = 50, 60 and 65 mol%) glasses should exhibit the properties of zero-stress birefringence.

Keywords: Silicate glasses; Pb^{2+} in glass; Structure; Neutron diffraction; RMC simulations; Stress-induced birefringence

1. Introduction

PbO has a wide glass forming range with several oxide materials such as B_2O_3 [1, 2], P_2O_5 [3], SiO_2 [4, 5], TeO_2 [6] and GeO_2 [7]. PbO acts as a network former at concentrations higher than 40 mol%, and as a network modifier at lower concentrations in xPbO–(100 − x)SiO_2 system [8]. The increase of PbO concentration in xPbO–(100 − x)SiO_2 system decreases the melting temperature and viscosity of the melt, while the density and refractive index of glasses increase significantly [9, 10]. The structural models of lead silicate glasses show that Pb^{2+} exist in PbO_x polyhedral units that are connected to each other and to SiO_4 tetrahedra, further it is known that the incorporation of PbO produces non-bridging oxygens (NBO) in the silicate network [11, 12]. Extended X-ray Absorption Fine Structure and molecular dynamics simulation studies by Rybicki and coworkers found that PbO_4 is the dominant Pb–O structural unit in lead silicate glasses [13, 14]. Pb–O bonds are significantly weaker than Si–O bonds, and the glass network can be easily depolymerized, resulting in a steady decrease of the glass transition temperature (T_g) with increase in PbO concentration [15].

Kohara et al. [16] studied the structure of lead silicate glasses by high-energy X-ray diffraction and Reverse Monte Carlo (RMC) simulations and concluded that the random network formation is governed by the interplay of SiO_4 and PbO_x polyhedra (x = 3, 4 and 5, and x = 4 as the major structural units). These researchers reported that there is inhomogeneous distribution of PbO_x units at low PbO concentration of 35 mol%, whereas at higher PbO concentration of 65 mol%, the SiO_4 units are inhomogeneously distributed in the glass network, and that the lead silicate glasses contain extraordinarily large amounts of free volume or voids in the glass network [16]. Glasses and crystalline materials with large concentration of voids can be used for storing Li^+ in the electrodes of secondary batteries [17–19].

*Corresponding author, E-mail: atul.phy@gndu.ac.in

Lead silicate glasses have several interesting and useful optical properties, Jia et al. found that these glasses are photosensitive and the optical absorption edge shifts toward longer wavelengths on exposure to ultraviolet radiation [20]. Bettinali and Ferraresso studied the low temperature luminescence properties of lead silicate glass and crystalline phases, and concluded that the light absorption and emission properties are due to electronic transitions of Pb^{2+} [21]. The two-photon absorption and nonlinear refraction has been reported in lead silicate glasses [22]. Lead metasilicate (50PbO-50SiO_2) melts show the intriguing effects of melt cooling rate on its crystallization properties [11].

Earlier we had investigated the mechanical, thermal, optical, vibrational spectra and devitrification properties of lead silicate glasses by X-ray diffraction, density, microhardness, dilatometry, differential scanning calorimetry (DSC), UV–visible and Raman spectroscopy [9]. It is the objective of the present work to elucidate the short-range structural properties i.e. Si–O, Pb–O, O–O bond lengths/nearest neighbor distances, coordination number and the bond angle distributions in xPbO–$(100 - x)SiO_2$ (x = 50, 60 and 65 mol%) glasses. The structural study is carried out by Reverse Monte Carlo (RMC) simulations of the neutron diffraction datasets. Neutrons are highly sensitive probes for investigating the oxygen–oxygen atomic pair correlations; which cannot be determined by X-rays due to the latter's weak scattering by low Z atoms (such as oxygen), therefore, neutron diffraction is the best technique to probe the atomic structure of oxide glasses.

The short-range structural properties of glasses have been used to predict the photoelastic properties (stress-induced birefringence) by the Zwanziger's model [23, 24], the latter is an empirical model that uses the cation-oxygen bond lengths (d), and the cation–anion coordination numbers (N_C) to predict the photoelastic properties. According to the Zwanziger model, the glass or a crystalline materials with the ratio $d/N_c > 0.50$, have negative stress-optic coefficients while those with $d/N_c < 0.50$ have positive stress-optic coefficients, while the materials with $d/N_c \sim 0.50$ are predicted to have zero-stress-optic properties [23, 24].

2. Experimental details

2.1. Glass preparation

Lead silicate glasses of the composition: xPbO–$(100 - x)SiO_2$ with x = 50, 60 and 65 mol% (hereafter referred to as 50PbSi, 60PbSi and 65PbSi, respectively) were prepared by using PbO (99.9%, Sigma-Aldrich Inc., India) and SiO_2 (99.9%, Fluka AG, Buchs, Switzerland) as starting materials. Chemicals were mixed together in appropriate molar ratios in an agate mortar pestle and then transferred to a platinum (Pt) crucible (20 cm^3). The batch mixture was sintered at 300 °C for 24 h and melted in the temperature range: 1000–1100 °C. The temperature of the Pt crucible containing the melt was measured by a chromel–alumel thermocouple positioned very close to it. For each composition, glass sample was prepared by the melt-quenching technique in which the melt was poured on a heavy brass plate and a disk shaped samples were obtained. To reduce thermal stresses, samples were immediately transferred to an oven where they were annealed at 400 °C for about 30 min and then cooled slowly to room temperature. Bubble free, transparent, yellow–brownish colored glasses were prepared for all the compositions and color of glasses darkened with increase in PbO concentration. Table 1 gives the composition, mass and atomic number densities of glasses.

2.2. Density measurements

The density of glass samples was determined by Archimedes principle on an electronic balance of sensitivity 10^{-4} g using dibutyl phthalate (DBP) as the immersion fluid. Measurement on each sample was done three to four times. The maximum error was ± 0.005 g cm^{-3} and the precision of measurements was better than 0.1% (Table 1).

2.3. Neutron diffraction experiments

Neutron diffraction studies of lead silicate glasses were carried out in the momentum transfer range, Q-range: 0.45 to 9.8 $Å^{-1}$for 24 h by using neutrons of de-Broglie wavelength, λ = 1.068 Å at the 2-axis PSD diffractometer of Budapest Neutron Center, Budapest, Hungary.

Table 1 Composition and densities of xPbO–$(100 - x)SiO_2$ (x = 50, 60 and 65 mol%) glasses

Sample code	Composition	Mass density (g· cm^{-3}) (± 0.005)	Atomic number density ($Å^{-3}$)
50PbSi	50PbO–50SiO_2	5.945	0.0632
60PbSi	60PbO–40SiO_2	6.668	0.0610
65PbSi	65PbO–35SiO_2	7.002	0.0596

Table 2 Neutron scattering weight factors (%) and cut-off distances for atom pairs used in the final RMC runs on lead silicate glasses

Atomic pairs	Weight factors, w_{ij} (%)			Cut-off distances, r_{ij} (Å)		
	50PbSi	60PbSi	65PbSi	50PbSi	60PbSi	65PbSi
Pb–Pb	9.22	13.37	15.81	2.90	2.80	2.90
Pb–Si	8.14	7.87	7.36	2.55	2.20	2.10
Pb–O	34.14	38.50	40.00	1.93	1.90	1.85
Si–Si	1.79	1.15	0.85	2.40	1.90	2.10
Si–O	15.07	11.30	9.40	1.35	1.10	1.25
O–O	31.63	27.70	25.90	1.90	1.75	1.80

The glass samples of mass, 3 to 4 g were pulverized into coarse powder and mounted in thin walled cylindrical vanadium can with a diameter of 8 mm for neutron diffraction measurements. The diffraction data were corrected for detector efficiency, background, multiple scattering, absorption effects and normalized with vanadium [25–28]. The total structure factor, $S(Q)$ was calculated by local software packages.

2.4. Reverse Monte Carlo (RMC) technique

RMC simulations were performed on experimentally measured total structure factor, $S(Q)$ to determine the short-range structural properties of glasses by using RMC ++ software [29, 30]. The RMC technique minimizes the square of the difference between the experimental $S(Q)$ and the calculated one from a three-dimensional atomic configuration by using the following equations [31–35]:

$$S(Q) = \sum_{i,j}^{k} w_{ij} S_{ij}(Q) \tag{1}$$

$$S_{ij}(Q) = 1 + \frac{4\pi\rho_o}{Q} \int_0^{r_{\max}} r\left[g_{ij}(r) - 1\right] \mathrm{Sin}Qr\mathrm{d}r. \tag{2}$$

The neutron scattering weight factors, w_{ij} for different atomic pair correlations were calculated by the following formulae [36–41]:

$$w_{ij}(Q) = \frac{c_i b_j c_j b_j \times \left(2 - \delta_{ij}\right)}{\left[\sum_i^k c_i b_i\right]^2} \tag{3}$$

where c_i, b_i are the molar fraction and coherent neutron scattering length of atoms of type i, $S_{ij}(Q)$ denotes the partial structure factors, and w_{ij} are the neutron scattering weight factors for the 6 atomic pairs: Pb–Pb, Pb–Si, Pb–O, Si–Si, Si–O and O–O (in these glasses $k = 3$, thus $k(k + 1)/2 = 6$ atomic pairs exist). The partial pair correlation functions $g_{ij}(r)$ for the above mentioned 6 atomic pairs were calculated, and these give the measure of the probability of finding the jth atom at a distance, r from the ith atom.

The following steps were used during RMC simulations to generate the partial atomic pair correlation function, $g_{ij}(r)$, the coordination numbers of the constituent atoms and three particle bond angle distributions:

(a) The simulation was started with a random initial configuration by building a box that contained 10,000 atoms of Pb, Si and O with the atomic density, ρ_o values of 0.0632 Å^{-3}, 0.0610 Å^{-3} and 0.0596 Å^{-3} for the three samples: 50PbSi, 60PbSi and 65PbSi, respectively (Table 1). The RMC model box lengths for the three samples were 27.03 Å, 27.36 Å and 27.57 Å, respectively.

(b) In the second step, the Pb, Si and O atoms were moved out by using the minimum interatomic distances constraints (cut-off distances) in the input program (Table 2). The tetrahedral coordination constraint was imposed on the first Si–O coordination sphere during the RMC simulations, and this condition was achieved up to a level of 98 to 99% during the RMC runs [42].

(c) RMC simulations were run, until the best fits between the calculated and experimental $S(Q)$ were obtained. Repeated RMC runs were performed to get reproducible data for each pair correlation, $g_{ij}(r)$, coordination number, CN_{ij} and bond angle distribution, θ (°).

The cut-off distances used in the final RMC run for Pb–Pb, Pb–Si, Pb–O, Si–Si, Si–O and O–O atom pairs for the three samples are given in Table 2.

Table 2 gives the input parameters namely the weight factors and the set of the cut-off distances, used in the final RMC run for the three glass samples. It can be seen that for the Pb–O and Si–O atomic pair correlation distributions, the weight factors have large values; which highlights the fact that neutron diffraction can provide reliable information for both the Pb and Si environments. The O–O

Table 3 Bond lengths/nearest neighbor distances in lead silicate glasses

Sample code	Bond lengths (Å)					
	Pb–O	Si–O	O–O	Pb–Pb	Pb–Si	Si–Si
50PbSi	2.59 ± 0.05	1.60 ± 0.01	2.47 ± 0.05	3.53 ± 0.05	3.53 ± 0.05	(i) 2.49 ± 0.05 (ii)3.05 ± 0.05
60PbSi	(i) 2.35 ± 0.05 (ii)2.59 ± 0.05	1.64 ± 0.02	2.35 ± 0.05	3.55 ± 0.05	3.60 ± 0.05	(i) 2.49 ± 0.05 (ii) 2.84 ± 0.05
65PbSi	(i) 2.25 ± 0.05 (ii) 2.59 ± 0.05	1.64 ± 0.01	(i) 2.35 ± 0.05 (ii) 2.45 ± 0.05	3.60 ± 0.05	3.60 ± 0.05	(i) 2.49 ± 0.05 (ii) 2.64 ± 0.05 (iii) 3.10 ± 0.05

correlations have the highest weight factors in the neutron diffraction experiments (Table 2), and therefore it was possible to obtain reliable O–O atomic pair correlation functions for all the samples, the latter are difficult to determine by X-ray diffraction studies.

The atomic pair correlation function, $g(r)$ (also known as the total pair correlation function in some literature [43, 44]) for each sample was calculated from the weighted sum of partial atomic pair correlation functions, $g_{ij}(r)$ by the following relationship [44, 45]:

$$g(r) = \sum_{i,j}^{k} w_{ij} g_{ij}(r) g(r) \tag{4}$$

where w_{ij} are the neutron scattering weight factors (Table 2) given by Eq. (3).

Table 3 gives the $r_{\min}$ and $r_{\max}$ values that were used to calculate the coordination numbers and bond angle distributions from the final RMC configuration file for each sample.

2.5. Atomic pair correlation functions by Fourier transformation

The atomic pair correlation function, $g(r)$ for each sample were also calculated by the Fourier sine transformation of the interference function, $F(Q) = Q(S(Q)-1)$ [45]:

$$g(r) = 1 + \frac{1}{2\pi^2 \rho_o r} \int_{Q_{\min}}^{Q_{\max}} F(Q) M(Q) \mathrm{Sin}(Qr) \mathrm{d}Q \tag{5}$$

where $M(Q)$ is the Lorch modification function defined as [16, 45–47]:

$$M(Q) = \frac{\mathrm{Sin}(\Delta Q)}{\Delta Q} \quad Q < Q_{\max} \tag{6}$$

$$M(Q) = 0 \quad Q > Q_{\max} \tag{7}$$

and $\Delta = \pi/Q_{\max}$, $Q_{\max}$ was selected around 10 Å^{-1} for determining $g(r)$ by (5).

3. Results and discussion

The RMC technique provided an excellent fit of the calculated structure functions ($S(Q) - 1$) with the experimental ones (Fig. 1). It is seen from Fig. 1 that there is a growth of the intensity of the first sharp diffraction peak (FSDP) in glasses on increasing PbO concentration from 50 to 65 mol%, the first glass sample: 50PbO-50SiO_2 (Sample Code: 50PbSi) has a broad shoulder at $Q = 1.26$ Å^{-1}, which grows into broad peak centered at 1.22 Å^{-1} with increase in PbO concentration to 60 mol% (Sample 60PbSi). Finally, the FSDP evolves into a well-defined peak centered at 1.20 Å^{-1} in the sample with 65 mol% PbO. The FSDP is correlated with the medium range order in glasses [48], and therefore the sharpening of FSDP indicates that the medium range order due to Pb–Pb, Pb–Si and Si–Si atomic correlations grow significantly with an increase in PbO concentration in glasses [49–51].

The RMC analysis successfully determined all the six atomic pair correlation functions in xPbO–(100 − x)SiO_2 glasses. Si–O distributions show peaks centered in the range of 1.60–1.64 ± 0.02 Å in all the three glasses (50PbSi, 60PbSi and 65PbSi). The Si–O atomic pair correlation functions (Fig. 2) are symmetrical although the width of these distributions increases significantly with the increase in Pb–O concentration from 50 to 65 mol%, and the Si–O bond-length is slightly higher for samples that contain 60 and 65 mol% PbO. The Pb–O pair correlation function (Fig. 3) is peaked at 2.60 ± 0.05Å in the glass with 50 mol% PbO, however the Pb–O atomic pair correlation distribution broadens significantly, and it shows at least two peaks centered at 2.25 ± 0.05 Å and 2.59 ± 0.05 Å in the sample containing 65 mol% PbO. Aldermann et al. studied the structure of xPbO–(100 − x)SiO_2 glasses by high energy X-ray diffraction and found that there are at least two types of Pb–O bonds in the lead silicate glass network, the shorter Pb–O bonds are at ∼ 2.2 Å and the longer ones are at ∼ 2.6 Å [51]. Similar results about the distribution of Pb–O bond

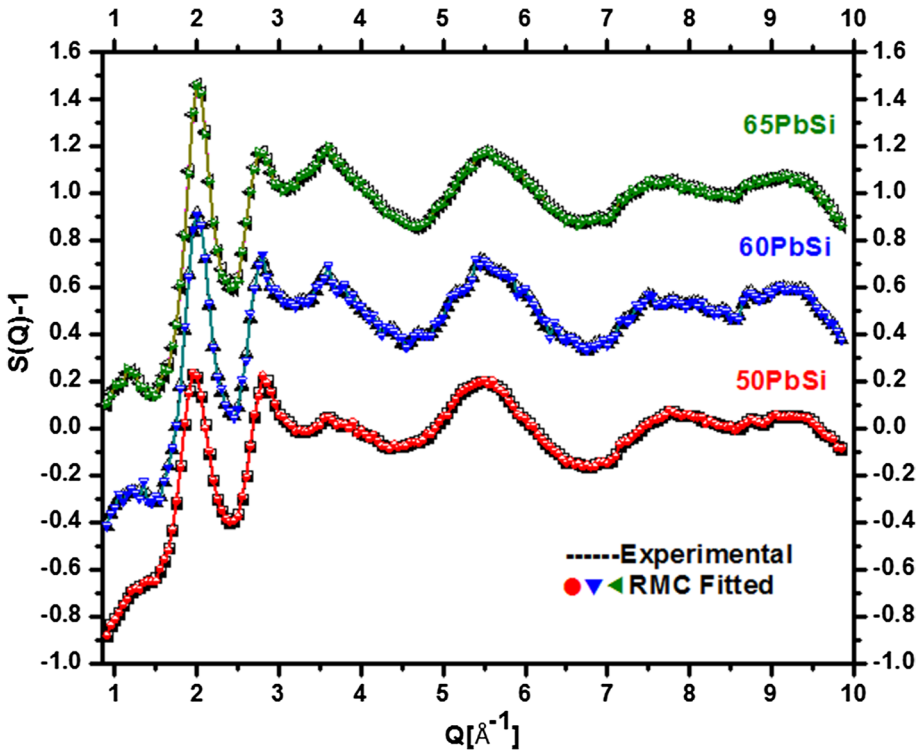

Fig. 1 Experimental and RMC calculated neutron structure factors. The graphs for the samples: 60PbSi and 65PbSi are displaced successively by 1 unit for clarity

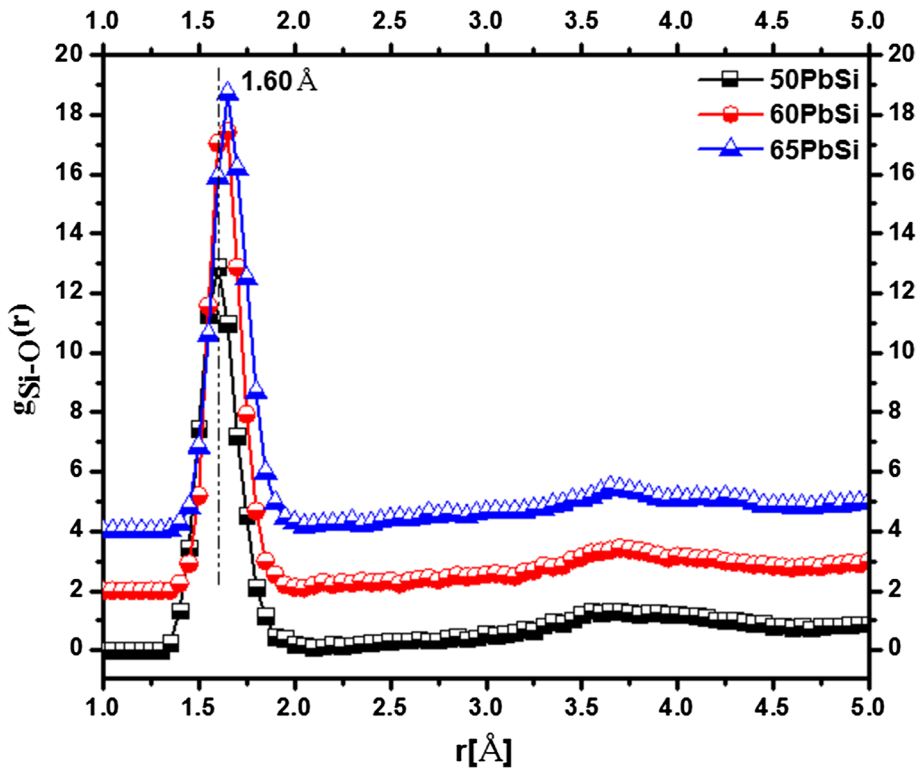

Fig. 2 Si-O pair correlation functions in xPbO–$(100 - x)SiO_2$ glasses determined by RMC simulations. Graphs for the samples 60PbSi and 65PbSi are displaced successively by 2 units for clarity

lengths were found from the neutron diffraction studies of xPbO-$(100 - x)TeO_2$ glasses [6]. Therefore it is concluded that the Pb–O bonds shorten with an increase in PbO concentration in the glass network.

The Pb–Pb atomic pair correlations (Fig. 4) show peaks at distances in the range of 3.53 to 3.60 ± 0.05 Å, similarly the Pb–Si correlations have peaks at the same distances in the range: 3.52 to 3.65 ± 0.05 Å (Fig. 5). Si–Si

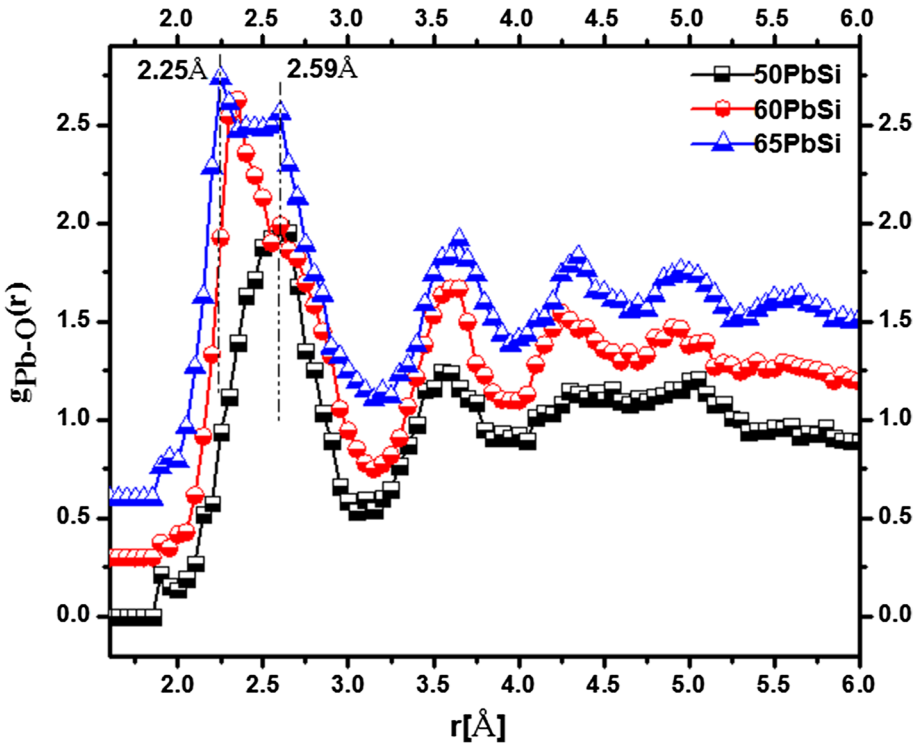

Fig. 3 Pb-O pair correlation functions in xPbO–$(100 - x)SiO_2$ glasses determined by RMC simulations. Graphs for the samples 60PbSi and 65PbSi are displaced successively by 0.3 units for clarity

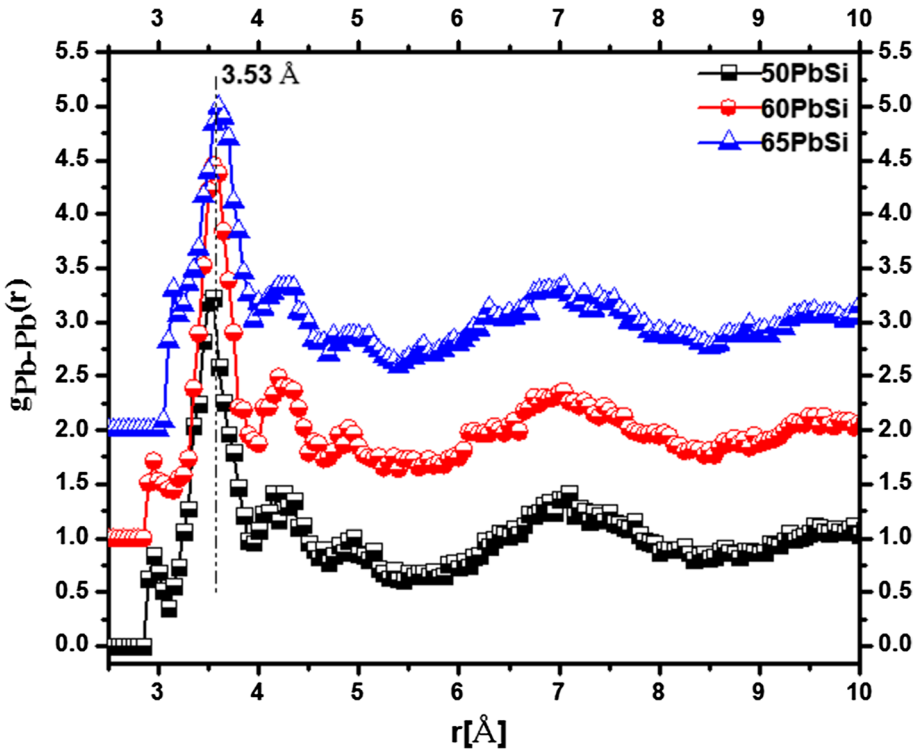

Fig. 4 Pb-Pb atomic pair correlation functions in xPbO–$(100 - x)SiO_2$ glasses determined by RMC simulations. Graphs for the samples 60PbSi and 65PbSi are displaced successively by 1 units for clarity

correlations show at least two broad maxima at 2.49 Å and 3.10 Å, the first peak in the Si–Si correlations shifts to smaller r-values (2.30-2.35 Å) on increasing PbO concentration to 60 and 65 mol% (Fig. 6). It may be noted that the neutron scattering weight factors for Si–Si linkages are quite small (1.79% to 0.85%) and hence the accuracy of the measurement of Si–Si distances is low. Finally, the nearest O–O distances are in the range of 2.35 Å to 2.49 ± 0.05 Å

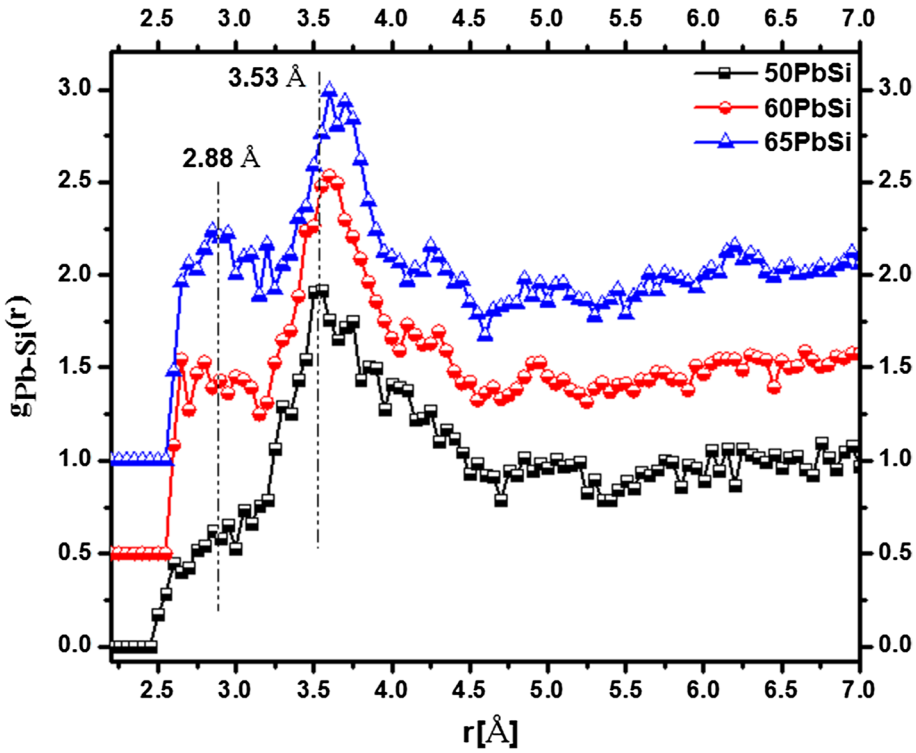

Fig. 5 Pb-Si atomic pair correlation functions in xPbO–$(100 - x)SiO_2$ glasses determined by RMC simulations. Graphs for the samples 60PbSi and 65PbSi are displaced successively by 0.5 units for clarity

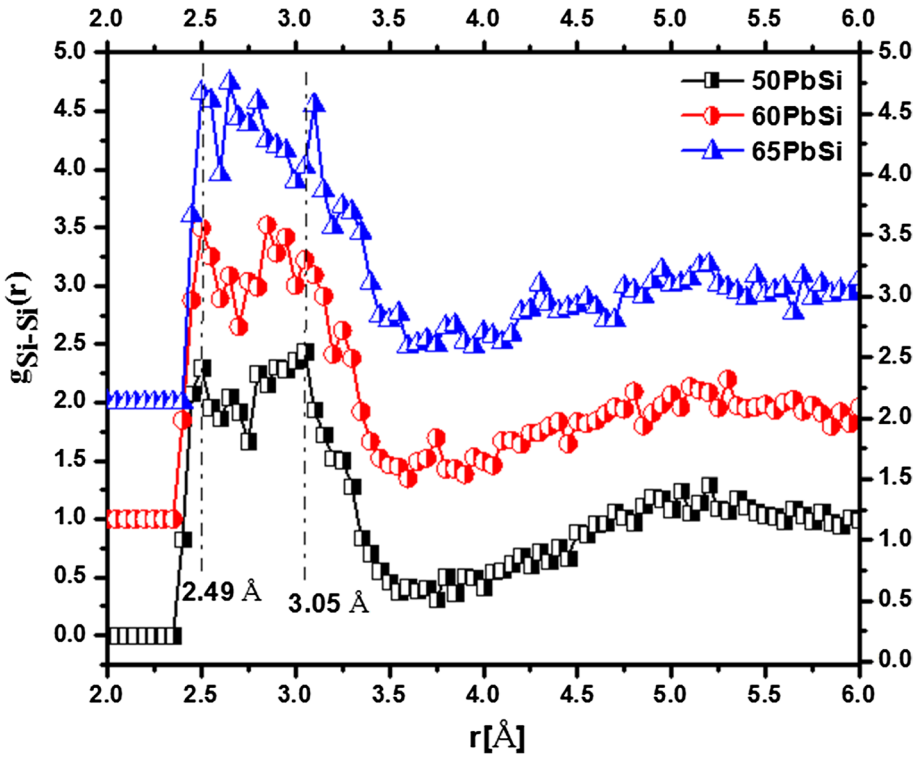

Fig. 6 Si-Si atomic pair correlation functions in xPbO–$(100 - x)SiO_2$ glasses determined by RMC simulations. Graphs for the samples 60PbSi and 65PbSi are displaced successively by 1 units for clarity

in the three lead silicate glasses (Fig. 7). Table 3 gives the values of bond lengths/nearest neighbor distances for the six atomic pairs in the glass series.

The atomic pair correlation function, g(r) for all the three samples was calculated from the weighted sum of partial atomic pair correlations determined by RMC analysis, and these are displayed in Fig. 8. The g(r) functions

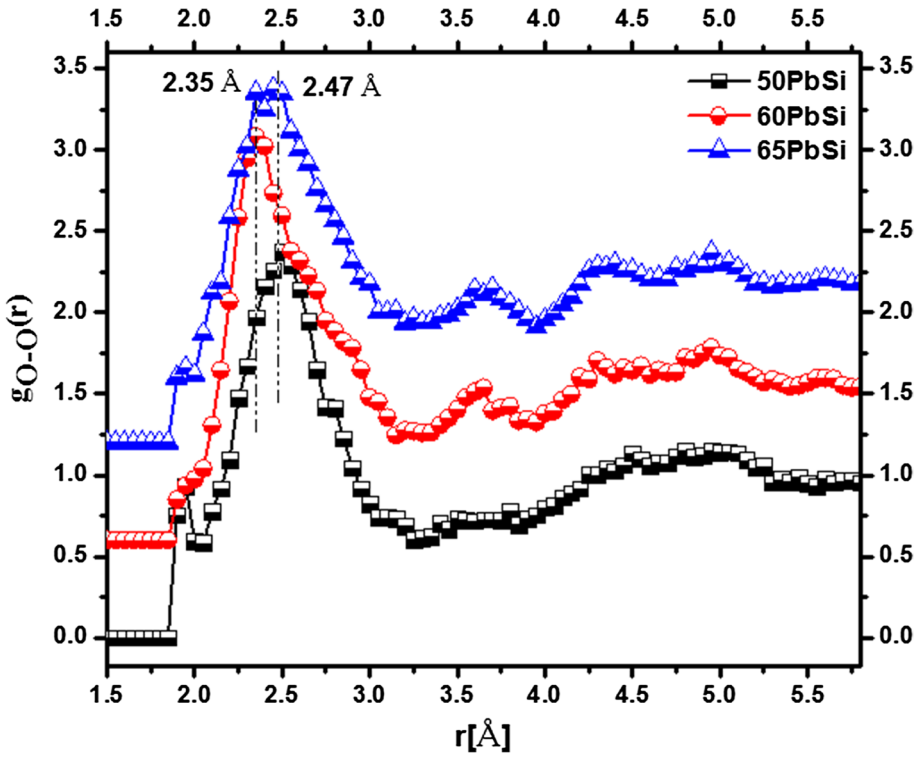

Fig. 7 O-O atomic pair correlation functions in xPbO–$(100 - x)SiO_2$ glasses determined by RMC simulations. Graphs for the samples 60PbSi and 65PbSi are displaced successively by 0.6 units for clarity

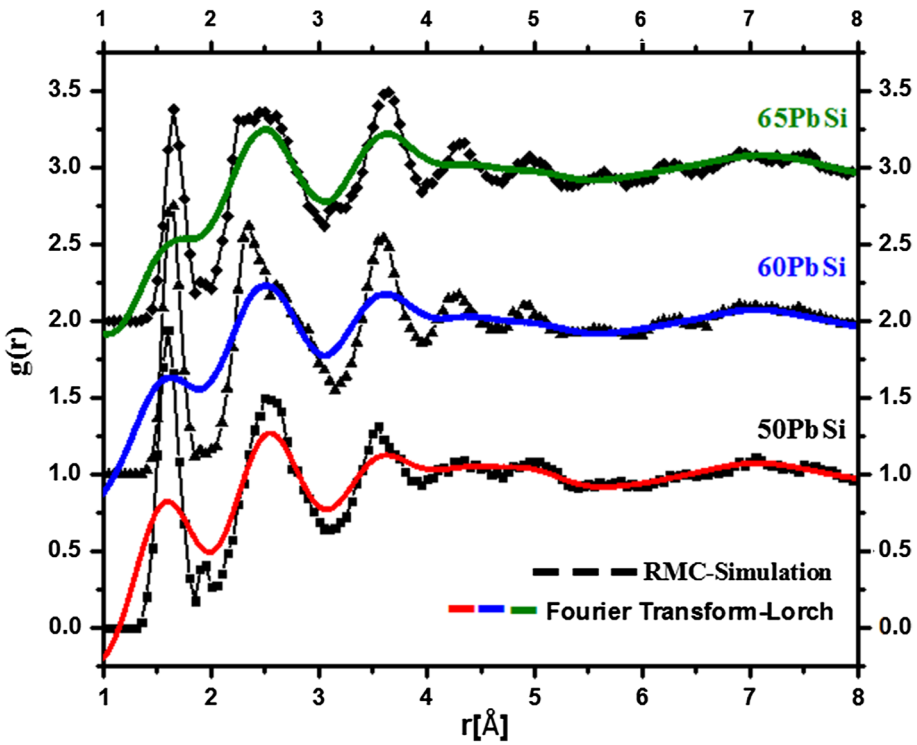

Fig. 8 Atomic pair correlation functions, g(r) in xPbO–$(100 - x)SiO_2$ glasses determined by RMC simulations (black) and Fourier transformation (colored). Graphs for the samples 60PbSi and 65PbSi are displaced successively by 1 unit for clarity

were also determined by the Fourier transformation of structure functions, S(Q) and their plots are shown in Fig. 8. The g(r) from Fourier transformation show peaks at exactly the same r-vales as in g(r) from the RMC analysis of the three samples, however the peaks due to different correlations are significantly sharper and better resolved in the g(r) by RMC technique. These results show that RMC method is very useful to obtain atomic pair correlation

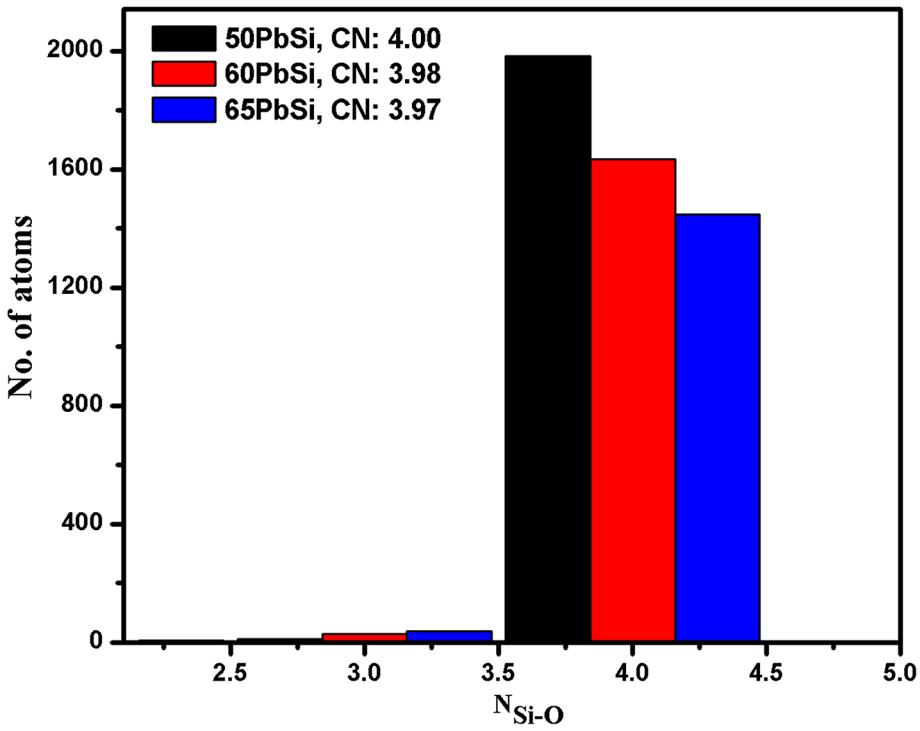

Fig. 9 Si–O coordination number (N_{Si-O}) distributions determined by RMC technique for the glasses: 50PbSi (black), 60PbSi (red) and 65PbSi (blue) (color figure online)

functions compared to the direct Fourier transformation, even with limited Q-range of neutron diffraction data.

The average Si–O coordination (N_{Si-O}) values were obtained from the RMC analysis of the neutron diffraction data, and it is found that Si^{4+} are tetrahedrally co-ordinated with oxygens in the lead silicate network and the coordination number is in the range: 3.97 ± 0.05 to 4.00 ± 0.05 (Fig. 9 and Table 4). The Pb–O coordination is in the range of 4.08 ± 0.11 to 4.14 ± 0.11 (Fig. 10), and therefore within the limits of experimental uncertainties, both Si–O and Pb–O coordination numbers are constant in the glass compositions that were characterized in this study. Kohara et al. reported Pb–O coordination of 4.2 in lead silicate glasses, and therefore our results show excellent agreement with the earlier findings [16]. The O–O coordination number is in the range: 5.59 ± 0.10 to 4.84 ± 0.08 (Fig. 11). Table 4 gives the r_{min} and r_{max} values that were used to calculate the coordination number and bond angle distributions from the final RMC configuration file for each sample.

The RMC simulations were used to determine the bond angle distributions. The O–Si–O bond angles show very broad distributions with maxima in the range of 109.1 ± 0.4° to 91.1 ± 1.1° (Fig. 12). It is clear that the O–Si–O bonds are distorted in the lead silicate glass network, and it deviates considerably from the ideal O–Si–O bond angle of 109.5° in the tetrahedral units. The large distortion of SiO_4 units in these glasses is probably due to the role of PbO as network former in these glasses, the strong interconnectivity of SiO_4 and PbO_x structural units [52] produces a distortion in the SiO_4 tetrahedron. The O–Pb–O (Fig. 13) and the O–O–O (Fig. 14) bond angles

Table 4 Average Pb–O, Si–O and O–O coordinations and bond angle distributions peak positions in lead silicate glasses (r_{min} and r_{max} values used to calculate the coordination numbers are given below each correlation)

Sample code	Average coordination number			Peak value of bond angle distribution (°)		
	N_{Pb-O} ($r_{min-}r_{max}$)	N_{Si-O} (r_{min} − r_{max})	N_{O-O} ($r_{min-}r_{max}$)	O–Pb–O	O–Si–O	O–O–O
50PbSi	4.08 ± 0.11	4.00 ± 0.05	5.59 ± 0.10	56.9 ± 1.0	97.4 ± 0.4	56.2 ± 0.6
	(1.82–3.15)	(1.31–2.09)	(1.84–3.25)	88.4 ± 1.0	109.1 ± 0.4	
60PbSi	4.14 ± 0.11	3.98 ± 0.05	4.85 ± 0.19	56.2 ± 0.1	91.1 ± 1.1	56.6 ± 0.9
	(1.82–3.15)	(1.34–2.04)	(1.82–3.15)	88.4 ± 0.1	109.1 ± 1.1	
65PbSi	4.14 ± 0.08	3.97 ± 0.06	4.84 ± 0.08	56.6 ± 1.2	91.0 ± 0.6	56.2 ± 0.3
	(1.82–3.15)	(1.35–2.05)	(1.82–3.20)	109.3 ± 1.2	97.7 ± 0.6	

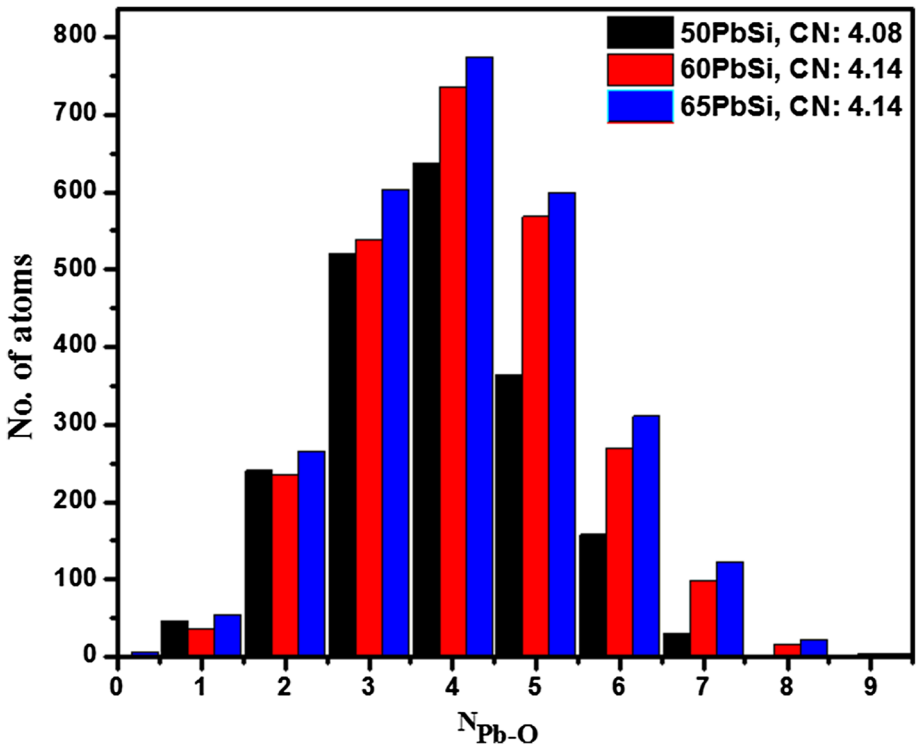

Fig. 10 Pb–O coordination number ($N_{Pb–O}$) distributions determined by RMC technique for the glasses: 50PbSi (black), 60PbSi (red) and 65PbSi (blue) (color figure online)

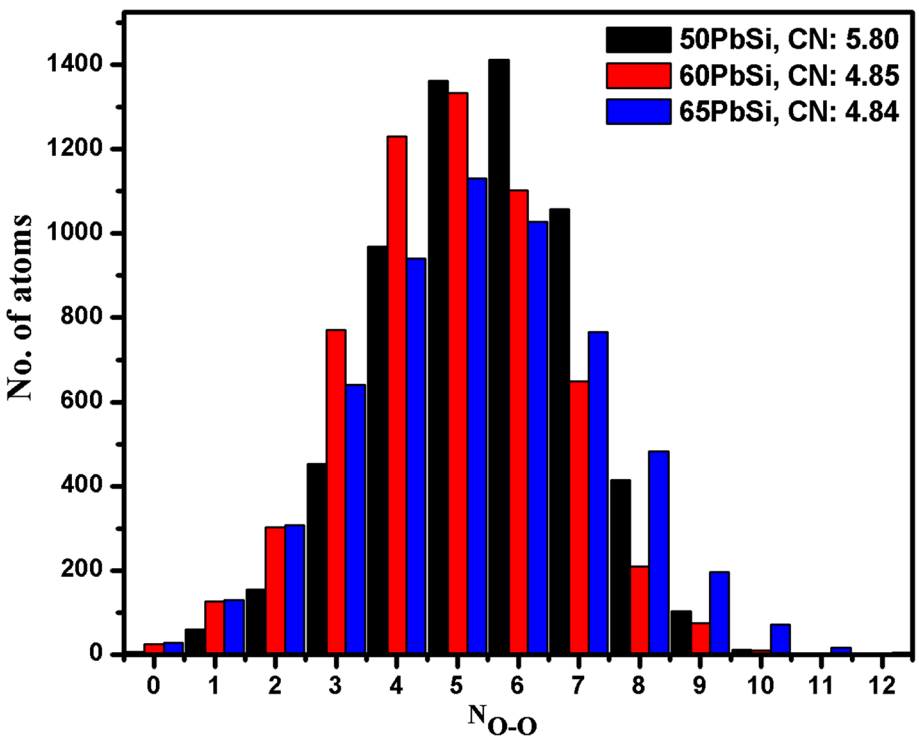

Fig. 11 O–O coordination number ($N_{O–O}$) distributions determined by RMC technique for the glasses: 50PbSi (black), 60PbSi (red) and 65PbSi (blue) (color figure online)

distributions show maxima in the same angle range of 56.2 ± 1.1° to 56.9 ± 1.0°.

The short-range structural properties of glasses i.e. Pb–O and Si–O bond lengths, Si–O and Pb–O coordination numbers were used in the Zwanziger model [23, 24], for predicting the photoelastic (stress-optic) response and the values of bonding characteristic, B_r were calculated by using the following empirical relationship [23, 24]:

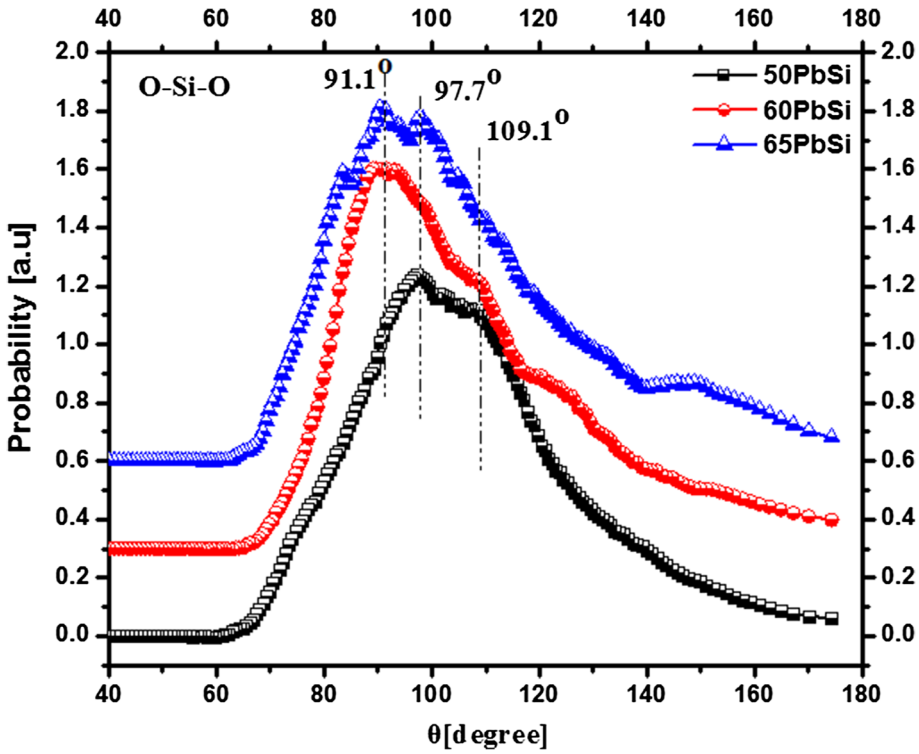

Fig. 12 O–Si–O bond angle distributions: 50PbSi (black), 60PbSi (red) and 65PbSi (blue) glasses. Curves for the samples 60PbSi and 65PbSi are successively displaced by 0.3 units for clarity (color figure online)

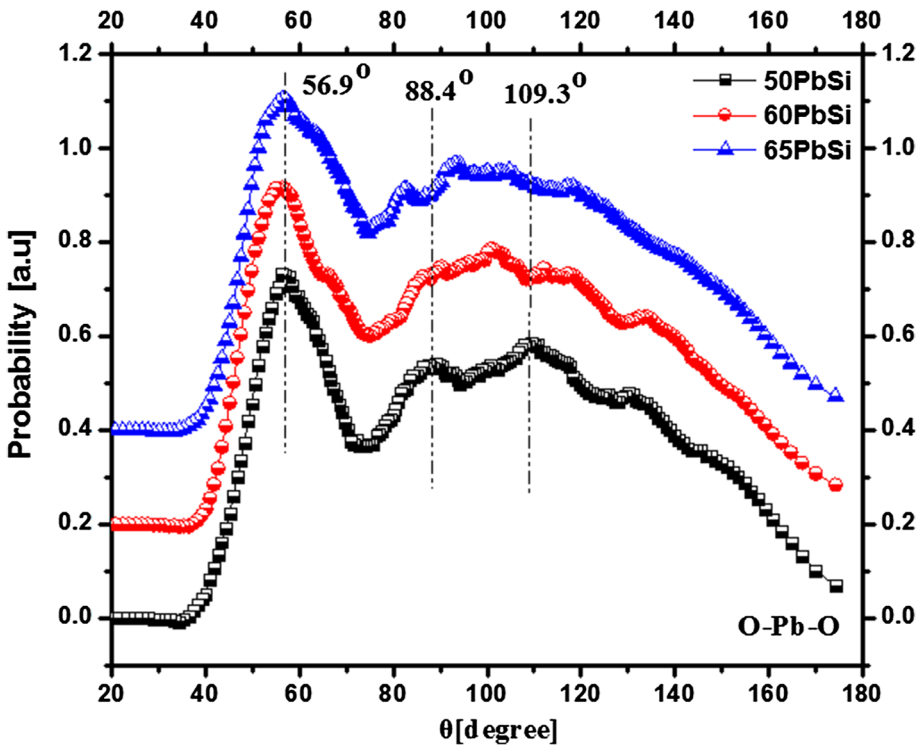

Fig. 13 O–Pb–O bond angle distributions in: 50PbSi (black), 60PbSi (red) and 65PbSi (blue) glasses. Curves for the samples 60PbSi and 65PbSi are successively displaced by 0.2 units for clarity (color figure online)

$$B_r = \sum_{i=1}^{n} x_i \left(\frac{d}{N_C}\right)_i . \quad (8)$$

It is found that B_r is 0.518 ± 0.033 Å, 0.522 ± 0.038 Å and 0.522 ± 0.033 Å in the glass samples: 50PbSi, 60PbSi and 65PbSi, respectively (Table 5). B_r values are equal within the limits of experimental uncertainties. It is predicted from empirical studies, that B_r of ~ 0.50 Å produces materials with zero-stress-induced birefringence [23, 24]. For example, it is known from experimental

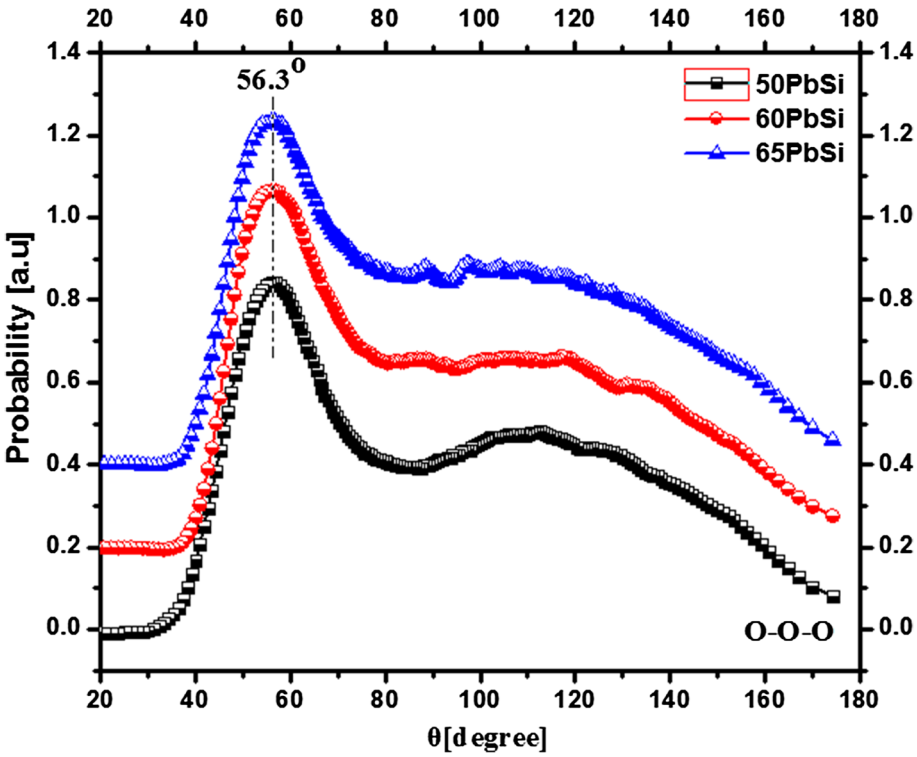

Fig. 14 O–O–O bond angle distributions in: 50PbSi (black), 60PbSi (red) and 65PbSi (blue) glasses. Curves for the samples 60PbSi and 65PbSi are successively displaced by 0.2 units for clarity (color figure online)

Table 5 Chemical bonding characteristic, B_r values in lead silicate glasses

Sample code	$<d_{(Pb-O)}>$ (Å)	$<d_{(Si-O)}>$ (Å)	d/N_C (Å) (Pb–O)	d/N_C (Å) (Si–O)	$B_r = \sum_{i=1}^{n} x_i \left(\frac{d}{N_C}\right)_i$ (Å)
50PbSi	2.59 ± 0.05	1.60 ± 0.01	0.637 ± 0.046	0.400 ± 0.019	0.518 ± 0.033
60PbSi	2.47 ± 0.05	1.64 ± 0.01	0.597 ± 0.047	0.412 ± 0.018	0.522 ± 0.038
65PbSi	2.42 ± 0.05	1.64 ± 0.01	0.584 ± 0.039	0.413 ± 0.019	0.524 ± 0.033

measurements that $17.5BaO–82.5TeO_2$ glass has zero-stress-optic properties (i.e. zero difference in the refractive indices along the axial and normal directions on applying stress on the glass sample). Neutron diffraction studies on $xBaO–(100 - x)TeO_2$ glasses [53] also predicted that oxide glasses with $B_r = 0.531 \pm 0.013$ Å should exhibit zero-stress birefringence (i.e. zero photoeleastic response). Crystalline α-TeO_2 with $B_r = 0.500$ Å is known to be a positive stress-optic response material [24], while crystalline α-Bi_2O_3 with $B_r = 0.55$ Å has negative stress-optic response [24], Similarly $xPbO–(100 - x)TeO_2$ ($x = 10$, 15 and 20 mol%) glasses have B_r values in the range of 0.535 Å to 0.547 Å and show negative stress-optic response [6]. Bechgaard concluded from photoelastic studies that lead borate glass with $B_r = 0.52$ Å should exhibit zero-stress-optic (photoelastic) properties [54]. Further, it was found by experimental measurements that $53PbO–47SiO_2$ glass exhibits zero-stress-optic properties [54, 55]. Therefore it can be concluded that lead silicate glasses containing 50 to 65 mol% of PbO, with B_r values in the range of 0.518–0.524 Å, are expected to show zero-stress-induced birefringence.

4. Conclusions

The short-range structural properties of three glasses: $50PbO–50SiO_2$, $60PbO–40SiO_2$ and $65PbO–35SiO_2$ were determined by the Reverse Monte Carlo (RMC) analysis of the neutron diffraction data. RMC simulations is an excellent technique to determine the glass short-range structure as it provides partial atomic pair correlation functions, accurate coordination environments and bond lengths which cannot be found from the Fourier transformation of the structure factors when there is strong overlapping of pair correlations.

Si^{4+} are tetrahedrally co-ordinated with oxygens and Pb^{2+} exist in variety of polyhedral units, however the average Si–O and Pb–O coordinations remain invariant in the glass series. The structural data were used to predict the

stress-optic (photoelastic) response of these glasses, and it is concluded that lead silicate glasses containing 50 to 65 mol% PbO should exhibit zero-stress-optic birefringence. These glasses are suitable for applications in flat panel displays that require materials that show minimum anisotropy of the optical properties with stress.

Acknowledgements Atul Khanna thanks UGC-DAE-Consortium for Scientific Research Indore and Mumbai Centers, and the Department of Science and Technology, New Delhi, India for research Grants that supported this work.

References

[1] D Mao and P J Bray *J. Non-Cryst. Solids* **144** 217 (1992)
[2] A Saini et al. *J. Non-Cryst. Solids* **355** 2323 (2009)
[3] B C Sales and L A Boatner *J. Am. Ceram. Soc.* **70** 615 (1987)
[4] L Zhang and S Jahanshahi *Metall. Mater. Trans. B* **29** 177 (1998)
[5] A M Zahra, C Zahra and B Piriou *J. Non-Cryst. Solids* **155** 45 (1993)
[6] A Kaur, H Hirdesh, A Khanna, M Fábián, P S R Krishna and A B Shinde *Mater. Res. Bull.* **110** 239 (2019)
[7] E M Rabinovich *J. Mater. Sci.* **11** 925 (1976)
[8] M Silva, Y Messaddeq, S J L Ribeiro, M Poulain, F Villain and V Briois *J. Phys. Chem. Solid* **62** 1055 (2001)
[9] A Kaur et al. *Phase Transit.* **86** 759 (2013)
[10] S Fujino, C Hwang and K Morinaga *J. Am. Ceram. Soc.* **87** 10 (2004)
[11] T Furukawa, S A Brawer and W B White *J. Mater. Sci.* **13** 268 (1978)
[12] P W Wang and L Zhang *J. Non-Cryst. Solids* **194** 129 (1996)
[13] A Rybicka, A Witkowska, G Bergmański, A Di Cicco, M Minicucci and G. Mancini *J. Phys. Condens. Matter* **13** 9781 (2001)
[14] A Witkowska, J Rybicki, S De Panfilis and A Di Cicco *J. Non-Cryst. Solids* **352** 4351 (2006)
[15] J M Jewell and J A Ruller *J. Non-Cryst. Solids* **152** 179 (1993)
[16] S Kohara et al. *Phys. Rev. B* **82** 134209 (2010)
[17] [17] S Afyon, F Krumeich, C Mensing, A Borgschulte and R Nesper *Sci. Rep.* **4** 7113 (2014)
[18] M Minakshi, N Sharma, D Ralph, D Appadoo and K Nallathamby *Electrochem. Solid-State Lett.* **14** A86 (2011)
[19] T Watcharatharapong, M M Sundaram, S Chakraborty, D Li, GM Shafiullah, R D Aughterson and R Ahuja *ACS Appl. Mater. Interfaces* **9** 17977 (2017)
[20] H Jia et al. *J. Non-Cryst. Solids* **319** 322 (2003)
[21] C Bettinali and G Ferraresso *J. Non-Cryst. Solids* **1** 91 (1968)
[22] Y Watanabe and T Tsuchiya *J. Non-Cryst. Solids* **210** 55 (1997)
[23] M Guignard and J Zwanziger *J. Non-Cryst. Solids* **353** 1662 (2007)
[24] M Guignard, L Albrecht and J Zwanziger *Chem. Mater.* **19** 286 (2007)
[25] A K Soper and P Egelstaff *Nucl. Instrum. Methods* **178** 415 (1980)
[26] Y Waseda, *The structure of non-crystalline materials: Liquids and amorphous solids*. McGraw-Hill, New York (1980)
[27] N Ramesh Rao, P S R Krishna, S Basu, B A Dasannacharya, K S Sangunni, E S R Gopal, *J. Non-Cryst. Solids* **240** 221 (1998)
[28] T Egami and S J Billinge *Underneath the Bragg Peaks: Structural Analysis of Complex Materials* (Amsterdam: Elsevier) (2003)
[29] G Evrard and L Pusztai *J. Phys. Condens. Matter* **17** S1 (2005)
[30] O Gereben, P Jóvári, L Temleitner and L Pusztai *J. Optoelectron. Adv. Mater.* **9** 3021 (2007)
[31] A Belushkin, V Y Kazimirov and S Manoshin *J. Non-Cryst. Solids* **402** 210 (2014)
[32] P Jóvári et al. *J. Am. Ceram. Soc.* **98** 1034 (2015)
[33] M Fábián and C Araczki *Physica Scripta* **91** 054004 (2016)
[34] M Fabian, E Svab and K Krezhov *J. Non-Cryst. Solids* **433** 6 (2016)
[35] P Jóvári et al. *J. Non-Cryst. Solids* **459** 99(2017)
[36] A Shikerkar, J A E Desa, P S R Krishna and R Chitra *J. Non-Cryst. Solids* **270** 234 (2000)
[37] H E Fischer, A C Barnes and P S Salmon *Rep. Prog. Phys.* **69** 233 (2005)
[38] I Kaban, P Jóvári, W Hoyer and E Welter *J. Non-Cryst. Solids* **353** 2474 (2007)
[39] J Dawidowski, J R Granada, J R Santisteban, F Cantargi and L A R Palomino *Experimental Methods in the Physical Sciences* (Amsterdam: Elsevier) 471 (2013)
[40] D L Price and F Fernandez-Alonso *Neutron Scattering-Magnetic and Quantum Phenomena* (Amsterdam: Elsevier) (2015)
[41] L Hennet, D H Moritz, R Weber and A Meyer *Experimental Methods in the Physical Sciences* (Amsterdam: Elsevier) 583 (2017)
[42] V Petkov and G Yunchov *J. Phys. Condens. Matter* **8** 1869 (1996)
[43] M Fábián, E Sváb, T Proffen and E Veress *J. Non-Cryst. Solids* **354** 3299 (2008)
[44] M Fábián, E Sváb, T Proffen and E Veress *J. Non-Cryst. Solids* **356** 441 (2010)
[45] M Eckersley, P Gaskell, A Barnes and P Chieux *J. Non-Cryst. Solids* **106** 132 (1988)
[46] E Lorch *J. Phys. C: Solid State Phys.* **2** 229 (1969)
[47] A K Soper and E R Barney *J. Appl. Crystallogr.* **45** 1314 (2012)
[48] S R Elliott *Nature* **354** 445 (1991)
[49] I Gee, D Holland and C McConville *Phys. Chem. Glasses* **42** 339 (2001)
[50] T Takaishi, M Takahashi, J Jin, T Uchino and T Yoko *J. Am. Ceram. Soc.* **88** 1591 (2005)
[51] O L Alderman et al. *Phys. Chem. Chem. Phys.* **15** 8506 (2013)
[52] I Vainshtein, A Zatsepin, V Kortov and Y V Shchapov *Phys. Solid State* **42** 230 (2000)
[53] A Kaur, A Khanna and M Fábián *Mater. Res. Express* **5** 065203 (2018)
[54] T K Bechgaard et al. *Opt. Mater.* **67** 155 (2017)
[55] M M Smedskjaer, M Potuzak, X Guo and J C Mauro *Opt. Mater.* **35** 2435 (2013)